A&A, 677, A55 (2023)
https://doi.org/10.1051/0004-6361/202346498
© The Authors 2023

Astronomy & Astrophysics

A new heavy anion in IRC +10216: Theory favors $C_{10}H^-$ versus C_9N^- ⋆

J. R. Pardo[1], C. Cabezas[1], M. Agúndez[1], B. Tercero[2,3], N. Marcelino[2,3], P. de Vicente[2,3], M. Guélin[4], and J. Cernicharo[1]

[1] Consejo Superior de Investigaciones Científicas, Instituto de Física Fundamental, Calle Serrano 121, 28006 Madrid, Spain
e-mail: jr.pardo@csic.es; jose.cernicharo@csic.es
[2] Centro de Desarrollos Tecnológicos, Observatorio de Yebes (IGN), 19141 Yebes, Guadalajara, Spain
[3] Observatorio Astronómico Nacional (OAN, IGN), Madrid, Spain
[4] Institut de Radioastronomie Millimétrique, 300 rue de la Piscine, 38406, Saint-Martin-d'Hères, France

Received 24 March 2023 / Accepted 26 June 2023

ABSTRACT

Continuing Q-band (31–50 GHz) integrations on IRC +10216 with the Yebes 40 m telescope have now reached sub-millikelvin noise with hundreds of new lines arising above an average 3σ detection limit of 0.71 mK (as low as 0.45 mK in the lower frequency end). The recent discovery of the C_7N^- anion and the relatively large abundance of the HC_9N member of the cyanopolyyne family opens the door for searching in the data for harmonically related series of lines belonging to singlet species, with intensities close to the detection limit, that could belong to heavier anions. One such series has been found with rotational quantum numbers from $J = 52 - 51$ up to $J = 74 - 73$, with at least 15 distinguishable features clearly detected as isolated or partly blended. There are two main candidates for the carriers of the series: C_9N^- and/or $C_{10}H^-$, for which our high-level-of-theory ab initio calculations predict a quite compatible rotational constant of ∼300 MHz. In this paper we discuss, based on our ab initio calculations and also on chemical models, which of these two candidates is the most likely carrier. There is more evidence for the $C_{10}H^-$ candidate. It would be, to date, the heaviest anion discovered in space through a series of detected individual lines.

Key words. molecular data – line: identification – stars: carbon – circumstellar matter – stars: individual: IRC+10216

1. Introduction

Following the initial overall publication of the ongoing Q-band line survey of IRC+10216, the envelope of the evolved star CW Leo, observed with the Yebes 40m telescope from May 2019 to February 2020 (Pardo et al. 2022), and other specific papers based on or making use of the same data set (Cernicharo et al. 2021a,b; Pardo et al. 2020, 2021; Changala et al. 2022) further observations were undertaken through the end of January 2023 that benefited from technical improvements in the receivers, resulting in better system temperatures. The noise in the current data set is therefore significantly reduced in comparison to the above cited publications (see Fig. 1). This opens new opportunities to identify rare species, such as anions (Cernicharo et al. 2023a).

The search for new molecules in astronomical sources currently requires extremely deep integrations as the list of known species increases. The new findings are not only important for extending the list of molecular species but also for the many questions arising from their presence in different astronomical environments, such as formation paths or physical conditions. Long molecules, ions, rare isomers, and high vibrational states are all being discovered as the sensitivity of the surveys reaches sub-millikelvin levels. Many of these new species are found only in the astronomical sources as their spectra are very difficult to reproduce in laboratory conditions. For this task, it is important to rely on constantly updated line catalogs that help us to focus on the unidentified features among an increasing forest of identified lines. Chemical models and other astronomical sources for reference or comparison are also valuable tools in the complex task of finding new species in space.

In this paper, we report on the discovery of a harmonically related series of lines toward IRC +10216 that we attribute to either C_9N^- or $C_{10}H^-$. In fact, the shorter counterparts of both anions (except C_2H^-) have been reported to be present in IRC+10216: CN^- (Agúndez et al. 2010), C_3N^- (Thaddeus et al. 2008), C_5N^- (Cernicharo et al. 2008, 2020a), C_7N^- (Cernicharo et al. 2023a), C_4H^- (Cernicharo et al. 2007), C_6H^- (McCarthy et al. 2006), and C_8H^- (Kawaguchi et al. 2007; Remijan et al. 2007).

The recent discovery of C_7N^- was based on lines with Yebes 40 m T_A^* intensities between 1 and 2 mK in IRC+12016. It is therefore expected that individual lines of C_9N^- or $C_{10}H^-$ will have peak intensities below 1 mK. The observations, data accumulation, and baseline fitting described in Sect. 2 are especially critical in this work. However, the noise in the final data products is low enough that no stacking technique has been necessary (see Sect. 3) as is the case in the TMC-1 detection reported by Remijan et al. (2023). The high level ab initio calculations performed for our task are presented in detail in Sect. 4, followed by a discussion on the identification of the carrier in Sect. 5. The chemical significance of the discovery for understanding the envelope of CW Leo, with comparisons to shorter similar anions

⋆ Based on observations carried out with the Yebes 40 m telescope (projects 19A010, 20A017, 20B014, 21A019) operated by the Spanish Geographic Institute (IGN, Ministerio de Transportes, Movilidad y Agenda Urbana).

Open Access article, published by EDP Sciences, under the terms of the Creative Commons Attribution License (https://creativecommons.org/licenses/by/4.0), which permits unrestricted use, distribution, and reproduction in any medium, provided the original work is properly cited.
This article is published in open access under the Subscribe to Open model. Subscribe to A&A to support open access publication.

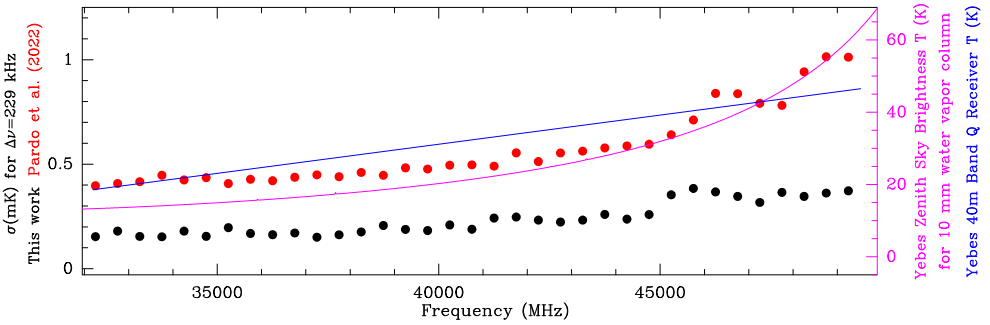

Fig. 1. Noise level in the spectra presented in this work at their final resolution (see Sect. 2) compared to data presented by Pardo et al. (2022). The typical atmospheric brightness temperature and average receiver temperature across the band are also plotted.

and neutral chains, is presented in Sect. 6. Finally, we present our final conclusions in Sect. 7.

2. Observations and data accumulation

The data presented in this paper are from an ongoing IRC+10216 Q-band (31–50 GHz) spectral survey within the framework of the Nanocosmos[1] project. The line survey accumulated 780 h of on-source observing time at each frequency in 250 observing sessions from May 2019 through the end of January 2023, with the 40 meter antenna of Yebes Observatory (IGN, Spain), (which we refer to as Yebes 40m throughout this paper). During this observational period, several improvements to the Nanocosmos equipment and the telescope were made. This large antenna now provides a main beam efficiency from 0.6 at 31 GHz to 0.43 at 50 GHz, and a beam size from 56″ to 36″ between those frequencies. Although the experimental setup was described in detail by Tercero et al. (2021), the most relevant information for this work is the use of a receiver consisting of two high-electron-mobility transistor (HEMT) cold amplifiers covering the 31.0–50.3 GHz band with horizontal and vertical polarizations. The backends are 16×2.5 GHz fast Fourier transform spectrometers (FFTSs), with a primary spectral resolution of 38.1 kHz, providing the whole coverage of the observed band in both polarizations.

The observing mode was position switching with an off position at 300″ in azimuth. The reference position used for IRC+10216 has been J2000 RA 09h47m57.36s Dec +13°16′44.4″. The HPBW of the antenna at 39.2 GHz is 45″. Pointing corrections were obtained by observing the SiO masers of R Leo, and errors were kept within 5″. The intensity scale of the final calibrated data is the antenna temperature (T_A^*) corrected for atmospheric absorption using the ATM package (Cernicharo 1985; Pardo et al. 2001). Calibration uncertainties are estimated to be within 10%.

The receiver temperature improvements during this long project, in addition to the changing atmospheric conditions and different integration times in each observing session, mean that adding of data must be cautiously undertaken if one is to obtain the best quality for the final spectrum. We used reference strong lines to discard whole (or parts of) observing sessions with technical or pointing problems. We then passed baselines to each FFTS section for each session after accumulating all valid scans (we avoided observations at very low elevations that would result in high noise). We then accumulated all sessions for each FFTS section, using the rms from the previous step as the weighting factor. We passed a new baseline to this result in smaller frequency ranges than the FFTS sections themselves in order to obtain a much finer treatment. We stored these smaller sections and finally stitched all of them together for the final spectrum. All of these steps were conducted without degrading the original spectral resolution (38 kHz). For the different publications, we applied a six-channel smoothing to the final spectrum. The spectral resolution in Fig. 2 is therefore 229 kHz.

[1] ERC grant ERC-2013-Syg-610256-NANOCOSMOS. https://nanocosmos.iff.csic.es/

3. Results

Line identification for this study made use of the catalogs MADEX (Cernicharo 2012), CDMS (Müller et al. 2005), and JPL (Pickett 1998). As of January 2023, the MADEX package contained 6464 spectral entries corresponding to the ground and vibrationally excited states, together with the corresponding isotopologues, of 1765 molecules. The new data of IRC +10216 have an unprecedented sensitivity level (see Fig. 1), reaching σ values as low as 0.15 mK on the T_A^* scale for a spectral resolution of 229 kHz.

The new data show a forest of unidentified lines, of which over 250 have been assigned to HC_9N in nv_{19} vibrational states from n = 1 up to 7. After a clear identification of these features it has been possible to detect several new molecules, such as C_7N^- (Cernicharo et al. 2023a), also detected in TMC-1 with the QUIJOTE line survey (Cernicharo et al. 2021a), HMgC-CCN, and NaCCCN (Cabezas et al. 2023), and, for the first time, the cationic species MgC_4H^+, MgC_3N^+, MgC_6H^+, and MgC_5N^+ (Cernicharo et al. 2023b).

As discussed by Cernicharo et al. (2023a), the detection of C_7N^- in IRC +10216 and TMC-1 suggests that the anions C_9N^- and $C_{10}H^-$ should be present in both sources. The starting point for our search was the rotational and distortion constants derived from the ab initio calculations described in Sect. 4. The expected rotational constant for both species is very similar, around ∼300 MHz. The lowest transition within the frequency range of our Q-band surveys of IRC +10216 and TMC-1 could be J = 52 − 51, with an estimated upper energy level of ∼40 K. We consequently focused our search on IRC+10216 as the intensity of the lines in TMC-1 is expected to be very low. A series of 15 lines was found in perfect harmonic relation with J_u from 52 up to 71. These lines are shown in Fig. 2 and their line parameters are presented in Table 1. A fit to the observed frequencies yields B = 299.8728 ± 0.0013 MHz and D = 1.14 ± 0.18 Hz. The standard deviation of the fit is 86 kHz.

Remijan et al. (2023) have recently reported, using line stacking techniques and lower frequencies, the detection of a new molecule in TMC-1 with B = 299.8713 MHz and D = 1 Hz (fixed value) that they assign to be $C_{10}H^-$. The rotational constant is in close agreement to the one we derived for our series of individually detected lines in IRC+10216. In fact, if we fix the distortion constant to 1 Hz, as the above authors did for the stacked data of TMC-1, the derived rotational constant for our series of IRC +10216 lines would be 299.87184±0.00017

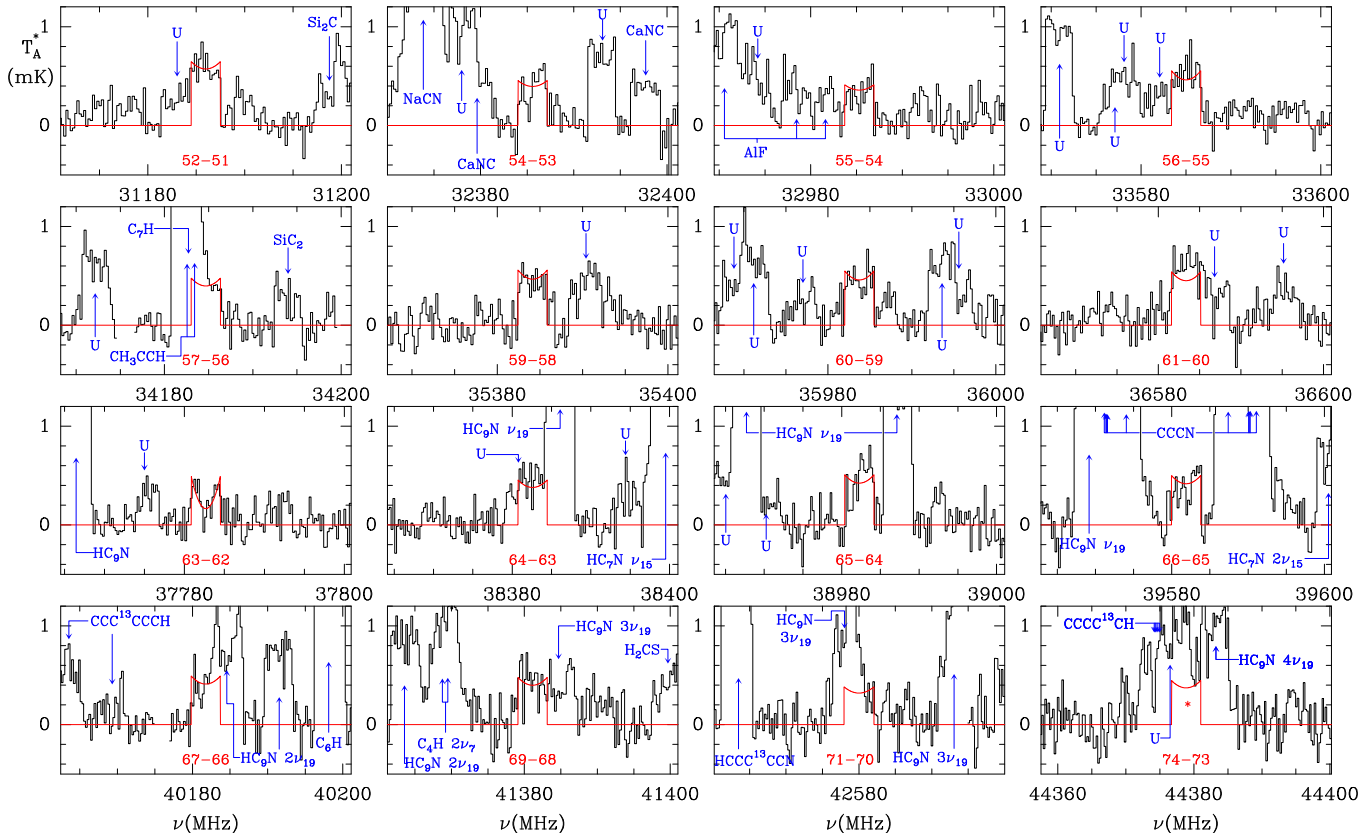

Fig. 2. New series of lines detected toward IRC+10216 in the *Q* band that could belong to C_9N^- or $C_{10}H^-$.

MHz, which agrees within 0.5 kHz with their value. We therefore conclude that we are dealing with the same species in both sources.

The detection of the same molecule in IRC +10216 and TMC-1 implies that we can discard vibrationally excited states and metal-bearing species as they are not expected at all in TMC-1. However, the assignment to $C_{10}H^-$ needs further discussion of alternative candidates since, for example, C_9N^- is predicted to have a very similar rotational constant: $B = 298.16$ MHz (see Table 2). Our high-level-of-theory ab initio calculations nevertheless favor the assignment to $C_{10}H^-$, for which a rotational constant of 299.63 MHz was calculated. Another species that should be considered is HC_8NC, for which the expected rotational constant varies between 296.3 MHz (Etim & Arunan 2017) and 311 MHz (Arnau et al. 1993) depending on the level of theory used in the calculations. The species HCCNC and HCCCCNC have been observed in TMC-1 (Cernicharo et al. 2020b). Hence, HC_6NC and HC_8NC could also be present in TMC-1. However, HCCCCNC is not observed in IRC +10216, and HC_6NC is not observed toward TMC-1 with the QUIJOTE line survey, nor toward IRC +10216 in the current ultrasensitive data set. Consequently, there is little chance that HC_8NC is the carrier of our lines. Similar arguments apply to other possible isomers of HC_9N. We therefore conclude that the most plausible carrier of our 15 lines is C_9N^- or $C_{10}H^-$, and discuss these two possibilities in detail in the following section.

4. Ab initio calculations

To obtain accurate rotational constants for C_9N^- and $C_{10}H^-$, we performed ab initio calculations. Similar calculations have been carried out for C_7N^- and C_8H^-, two species with the closest molecular structures for which the rotational parameters are experimentally available. In this manner, we can scale the calculated values for C_9N^- and $C_{10}H^-$ using experimental/theoretical ratios derived for the shorter and better known counterparts. We have also explored a few other possibilities. For example, the B constant obtained for C_9N^- when the results are scaled from HC_9N is 298.5 MHz, very close to the value obtained with C_7N^- as reference (298.4 MHz).

The geometry optimization calculations for all the species were undertaken using the coupled cluster method with single, double, and perturbative triple CCSD(T) excitations (Raghavachari et al. 1989) together with Dunning's correlation consistent polarized valence triple-ζ (cc-pVTZ; Woon & Dunning 1993) method. With the optimized geometry, the electric dipole moment was calculated at the same level of theory as that for the geometrical optimization. These calculations were carried out using the MOLPRO package (version 2020.2; Werner et al. 2012). The values for the centrifugal distortion constants were obtained using harmonic vibrational frequency calculations, with, respectively, the second order Møller-Plesset (MP2) perturbation theory method (Møller & Plesset 1934) and the correlation consistent with the polarized valence triple-ζ basis set (cc-pVTZ; Woon & Dunning 1993). These calculations were carried out using the Gaussian16 program (Frisch et al. 2016).

Table 2 shows the results obtained for C_9N^- and $C_{10}H^-$, for which the rotational and centrifugal distortion constants were scaled using the experimental/theoretical ratio obtained for the corresponding parameter of C_7N^- and C_8H^-, respectively. The calculated values of the dipole moment are 15.2 D and 10.0 D for $C_{10}H^-$ and C_9N^-, respectively.

Table 1. Observed line parameters of the new molecule toward IRC +10216.

J_u	ν_{obs} [a] (MHz)	$\Delta\nu$ [b] (MHz)	$\int T_A^* dv$ [c] (mK km s^{-1})	T_A^* [d] (mK)	Blended with
52	31186.014±0.100	–0.133	17.26	0.65/0.57	
53	31785.852[*]				C_4H ν_7
54	32385.582±0.100	0.027	12.00	0.45/0.40	
55	32985.308±0.100	0.051	10.92	0.41/0.36	
56	33585.009±0.100	0.052	14.25	0.55/0.46	
57	34184.681±0.100[+]	0.026	12.29	0.48/0.40	C_7H & CH_3CCH
58	34784.352[*]				MgC_6H
59	35384.140±0.100	0.093	14.37	0.56/0.47	
60	35983.740±0.100	0.001	14.13	0.55/0.46	
61	36583.364±0.100	–0.067	13.90	0.54/0.45	
62	37183.120[*]				HC_9N & CH_3CN
63	37782.673±0.100	-0.135	7.90	0.49/0.16	
64	38382.592±0.200[+]	0.099	11.69	0.45/0.37	HC_9N ν_{19}
65	38982.276±0.200	0.099	13.04	0.51/0.42	
66	39581.880±0.200	0.022	12.89	0.50/0.42	
67	40181.770±0.300	0.232	12.65	0.49/0.41	
68	40781.215[*]				HC_9N $2\nu_{19}$
69	41381.126±0.200	0.236	12.29	0.48/0.40	
70	41980.564[*]				U line
71	42580.010±0.200[+]	–0.226	9.83	0.38/0.32	HC_9N $3\nu_{19}$
72	43179.904[*]				U line
73	43779.570[*]				U line
74	44379.234[*]				HC_9N $2\nu_{19}$ & $CCCC^{19}CH$

Notes. [a]Observed frequency assuming a v_{LSR} of –26.5 km s^{-1}. [b]Observed minus calculated frequencies in MHz. [c]Integrated line intensity in mK km s^{-1}. Uncertainty is assumed to be dominated by the calibration uncertainty of 10%. [d]Antenna temperature at the terminal velocity (horn) and at the line center in millikelvin (mK). [+]Blended line but fit still possible. [*]Heavily blended. Fit not possible. Reported frequency corresponds to the predicted one.

Table 2. Spectroscopic parameters B (MHz) and D (Hz) for C_9N^- and $C_{10}H^-$ species.

	C_7N^-		C_9N^-	
Parameter	Calc. [a]	Exp. [b]	Calc. [a]	Scaled [a]
B	579.60	582.6849	296.59	298.16
D	3.7	4.00	0.757	0.85
	C_8H^-		$C_{10}H^-$	
Parameter	Calc. [a]	Exp. [c]	Calc. [a]	Scaled [a]
B	580.02	583.3401	297.92	299.63
D	3.68	4.285	0.76	0.89

Notes. [a]This work. [b]Cernicharo et al. (2023a). [c]Gupta et al. (2007).

It should be noted that the calculations provide the equilibrium values for the rotational constant (B_e), while the experimental values are the ground state rotational constants (B_0). Despite the equilibrium rotational constants being slightly different from the ground state constants, we can assume similar discrepancies for the target species and their respective references, C_9N^- and C_7N^- and C_8H^- and $C_{10}H^-$. Hence, the estimated constants for both species are essentially unaffected by this. An example of this can be seen for C_7N^- and HC_7N species, with the difference between the calculations based upon whether or not the vibration-rotation corrections are around 0.07% (Cabezas et al. 2022).

5. Discussion. C_9N^- or $C_{10}H^-$?

Our calculations (presented in the previous section) favor the assignment of the series of lines observed in IRC +10216 and TMC-1 to $C_{10}H^-$, for which the difference between the predicted and observed value of the rotational constant is 0.25 MHz (0.1%), while for C_9N^- it is higher, 1.8 MHz (0.6%). However, we need further arguments to discard the latter species.

The detection of C_7N^- in IRC +10216 (Cernicharo et al. 2023a) indicates that C_9N^- and $C_{10}H^-$ could have similar abundances with a column density that could be between a few 10^{11} and 10^{12} cm^{-2}. From the calculated dipole moments and assuming identical column densities and excitation conditions, the intensity of the lines of C_9N^- would be 2.3 times weaker than those of $C_{10}H^-$, which is below the sensitivity of our present Q-band IRC+10216 data. Inversely, if the carrier of the lines was C_9N^-, then the intensity of the lines of $C_{10}H^-$ would be 2.3 times stronger than those observed and easily detected in our data.

We have carefully explored the data, searching for a rotational constant between 295 and 305 MHz. No other series of lines with similar or stronger intensities than those observed was found. Hence, assuming identical column densities for both anions, as is the case for C_7N^- and C_8H^- in IRC +10216 (Cernicharo et al. 2023a), it is tempting to definitively assign the lines to $C_{10}H^-$.

We constructed a rotation diagram using the velocity-integrated line intensities presented in Table 1 and assuming an emission size with a radius of 15″, as observed for different neutral carbon chains in IRC +10216 (e.g., Agúndez et al. 2017). The rotational temperature is found to be 27.3 ± 1.9 K. The column density derived is $(4.4 \pm 0.7) \times 10^{11}$ cm^{-2} if the carrier is $C_{10}H^-$ or $(1.00 \pm 0.15) \times 10^{12}$ cm^{-2} if the carrier is C_9N^-.

We searched for the previously known lines of $C_{10}H$ (Gottlieb et al. 1998) with no positive results for any of them in the Q-band. Adopting a dipole moment of 7.5 D and a rotational temperature identical to that of $C_{10}H^-$, we derive an upper limit to the column density of $C_{10}H$ of 1.5×10^{11} cm^{-2}.

6. Chemical models

To shed some light on the formation of anions in IRC +10216 and on the expected relative abundances between them, we carried out chemical modeling calculations. We used the chemical model constructed by Agúndez et al. (2017) to elucidate the growth mechanism of carbon chains in IRC +10216, which was validated against ALMA observations. We expanded the chemical network to include carbon chains C_n, C_nH, HC_nH, C_mN, and HC_mN, and the related anions C_n^-, C_nH^-, and C_mN^- up to $n = 20$ and $m = 19$. The main formation route to anions is radiative electron attachment to the neutral counterpart, for which we adopted the rate coefficients calculated by Herbst & Osamura (2008) for C_nH with n = 2–8, while for n = 9,10 we used the values calculated by Millar et al. (2007), and assumed the value of $n = 10$ for $n > 10$. For the nitriles, we adopted the value calculated by Petrie & Herbst (1997) for C_3N and a rate coefficient of $1.25 \times 10^{-7} (T/300)^{-0.5}$ cm^3 s^{-1} for C_mN with $m \geq 5$,

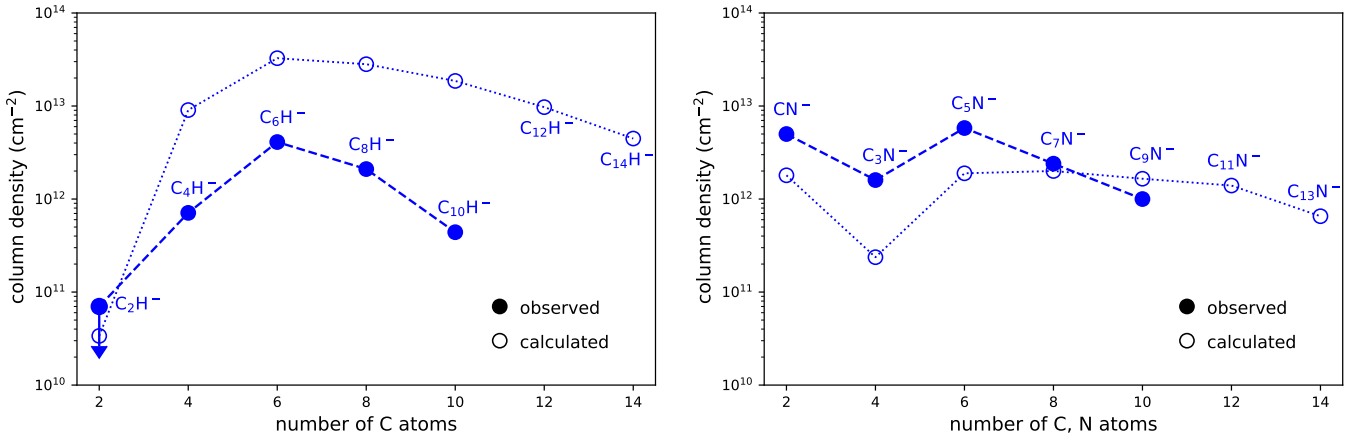

Fig. 3. Column densities of negative ions calculated with the chemical model compared with observed values. The left panel shows hydrocarbon anions, while the right panel shows nitrile anions. The observed values for $C_{10}H^-$ and C_9N^- were derived assuming that they are the carriers of the series of lines reported in this work.

as given for C_5N in Walsh et al. (2009). The main destruction mechanism of anions is the reaction with H atoms, for which we adopted the rate coefficients measured by Eichelberger et al. (2017). We also included, as destruction mechanisms, reactions of either O or N atoms with abundant cations, and photodetachment.

In Fig. 3, we compare column densities calculated by the chemical model with the values derived from the observations. Calculated values are given as radially integrated column densities, which are expected to provide a first order estimate of the true column density. For a more detailed estimate, one should take into account the role of excitation through collisions with H_2 and infrared pumping. The absolute column densities and the trends with increasing size found are roughly similar to those of previous chemical models of IRC+10216 (e.g., Millar et al. 2000; Cordiner & Millar 2009). We first note that calculated column densities for C_nH^- anions are approximately one order of magnitude higher than the observed values. Excitation may be largely responsible for this difference. In the case of C_mN^- anions, calculated and observed column densities agree better. The most interesting information that can be obtained from the chemical model is perhaps how the column density varies as the size of the anion increases. In the case of the hydrocarbon anions C_nH^-, the chemical model and the observations are in agreement that the maximum column density is reached for C_6H^- and then the column density decreases as the size of the anion increases. According to the chemical model, the column density ratio $C_8H^-/C_{10}H^-$ is 1.5, while, if the carrier of the line series reported in this paper is $C_{10}H^-$, the observed value of the same ratio would be 4.8. In the case of the nitrile anions C_mN^-, the chemical model reproduces the observed trend rather well, in which CN^- is quite abundant, then C_3N^- is present at a lower level, and C_5N^- again increases in abundance. The observations then indicate that the column density decreases with increasing size, while the chemical model predicts a less steep decline. The chemical model predicts a column density ratio C_7N^-/C_9N^- of 1.2, while, if the carrier of our series of lines is C_9N^-, this ratio would be 2.4. The chemical model would then be consistent with either $C_{10}H^-$ or C_9N^- as the carrier of the reported series of harmonically related lines. In fact, both anions are expected to be present in IRC+10216 with abundances slightly smaller than the corresponding smaller counterparts, C_8H^- and C_7N^-, respectively.

7. Conclusions

We report the detection of 15 harmonically related lines in IRC+10216 for which we derive B = 299.8728 ± 0.0013 MHz and D = 1.14 ± 0.18 Hz. The rotational constant agrees within 1σ with the value derived from a stacking statistical analysis of the GOTHAM TMC-1 data (Remijan et al. 2023). These authors assign the carrier to $C_{10}H^-$. However, other species, in particular C_9N^-, could have a very similar rotational constant. We have performed high-level-of-theory ab initio calculations that yielded $B(C_9N^-)$ = 298.16 MHz and $B(C_{10}H^-)$ = 299.63 MHz with an expected accuracy better than 0.1%. These calculations therefore favor $C_{10}H^-$ as the carrier of the reported individual lines in IRC+10216 and of the line stacking analysis of the GOTHAM TMC-1 line survey. Chemical models nevertheless predict that both anions should be detectable in both sources. A careful search within our present IRC+10216 Q-band data for series of lines with B between 295 and 305 MHz has provided negative results at the present level of sensitivity. We thereby conclude that the most likely carrier of the reported lines is $C_{10}H^-$. A definitive conclusion would require laboratory work on both anions.

Acknowledgements. We thank Ministerio de Ciencia e Innovación for funding support through projects PID2019-106110GB-I00, PID2019-107115GB-C21, and PID2019-106235GB-I00. We also thank ERC for funding through grant ERC-2013-Syg-610256-NANOCOSMOS.

References

Agúndez, M., Cernicharo, J., Guélin, M., et al. 2010, A&A, 517, A12
Agúndez, M., Cernicharo, J., Quintana-Lacaci, G., et al. 2017, A&A, 601, A4
Arnau, A., Silla, E., & Tuñon, I. 1993, ApJ, 415, L151
Cabezas, C., Agúndez, M., Marcelino, N., et al. 2022, A&A, 659, A8
Cabezas, C., Pardo, J. R., Agúndez, M., et al. 2023, A&A, 672, L12
Cernicharo, J. 1985, Internal IRAM report (Granada: IRAM)
Cernicharo, J. 2012, in ECLA 2011: Proc. of the European Conference on Laboratory Astrophysics, EAS Publications Series, 2012, eds. C. Stehl, C. Joblin, & L. d'Hendecourt (Cambridge: Cambridge University Press), 251 https://nanocosmos.iff.csic.es/?page$_$id=1619
Cernicharo, J., Guélin, M., Agúndez, M., et al. 2007, A&A, 467, L37
Cernicharo, J., Guélin, M., Agúndez, M. et al. 2008, ApJ, 688, L83
Cernicharo, J., Marcelino, N., Pardo, J. R., et al. 2020a, A&A, 641, A9
Cernicharo, J., Marcelino, N., Agúndez, M., et al. 2020b, A&A, 642, A8
Cernicharo, J., Agúndez, Cabezas, C., et al. 2021a, A&A, 649, L15

Cernicharo, J., Agúndez, Kaiser, R. I., et al. 2021b, A&A, 652, A9
Cernicharo, J., Pardo, J.R., Cabezas, C., et al. 2023a, A&A, 670, A19
Cernicharo, J., Cabezas, C., Pardo, J. R., et al. 2023b, A&A, 672, L13
Changala, P. B., Gupta, H., Cernicharo, J., et al. 2022, ApJ, 940, L42
Cordiner, M. A., & Millar, T. J. 2009, ApJ, 697, 68
Eichelberger, B., Snow, T. P., Barckholtz, C., & Bierbaum, V. M. 2007, ApJ, 667, 1283
Etim, E. E., & Arunan, E. 2017, Astrophys. Space Sci., 362, 4
Frisch, M. J., Trucks, G. W., Schlegel, H. B., et al. 2016, Gaussian 16 Revision A.03
Gottlieb, C. A., McCarthy M. C., Travers M. J., et al. 1998, J. Chem. Phys. 109, 5433
Gupta, H., Brünken, S., Tamassia, F., et al. 2007, ApJ, 655, L57
Herbst, E., & Osamura, Y. 2008, ApJ, 679, 1670
Kawaguchi, K., Fujimori, R., Aimi, S. 2007, PASJ, 59, L47
McCarthy, M. C., Gottlieb, C. A., Gupta, H., et al. 2006, ApJ, 652, L141
Millar, T. J., Herbst, E., & Bettens, R. P. A. 2000, MNRAS, 316, 195
Millar, T. J., Walsh, C., Cordiner, M. A., et al. 2007, ApJ, 662, L87
Møller, C., & Plesset, M. S. 1934, Phys. Rev., 46, 618
Müller, H. S. P., Schlöder, F., Stutzki, J., & Winnewisser, G. 2005, J. Mol. Struct., 742, 215
Pardo, J. R., Cernicharo, J., & Serabyn, E. 2001, IEEE Trans. Antennas Propag., 49, 12
Pardo, J. R., Bermúdez, C., Cabezas, C., et al. 2020, A&A, 640, L13
Pardo, J. R., Cabezas, C., Fonfría, J. P., et al. 2021, A&A, 652, L13
Pardo, J. R., Cernicharo, J., Tercero, B., et al. 2022, A&A, 658, A39
Petrie, S., & Herbst, E. 1997, ApJ, 491, 210
Pickett, H. M., Poynter, R. L., Cohen, E. A., et al. 1998, JQSRT, 60, 883
Remijan, A. J., Hollis, J. M., Lovas, F. J., et al. 2007, ApJ, 664, L47
Raghavachari, K., Trucks, G. W., Pople, J. A., & Head-Gordon, M. 1989, Chem. Phys. Lett., 157, 479
Remijan, A. J., Scolati, H. M., Burkhardt, A. M., et al. 2023, ApJ, 944, L45
Thaddeus, P., Gottlieb, C. A., Gupta, H., et al. 2020, ApJ, 677, 1132
Tercero, F., López-Pérez, J. A., Gallego, J. D., et al. 2021, A&A, 645, A37
Walsh, C., Harada, N., Herbst, E., & Millar, T. J. 2009, ApJ, 700, 752
Werner, H.-J., Knowles, P.-J., Knizia, G., Manby F. R., & Schütz, M. 2012 WIREs Comput. Mol. Sci. 2, 242
Woon, D. E., & Dunning, T. H., Jr. 1993, J. Chem. Phys., 98, 1358